Experimental study on evaporation characteristics of light cycle oil (LCO) droplet under various ambient conditions

Yushin Naito,[†] Kengo Ueda [†] Nozomu Hashimoto,[,†] Masahide Takagi,[‡]*

Satoshi Kawauchi,[‡] Yasuo Imai,[‡] Manabu Watanabe,[§] Takayuki Hasegawa,[§] Toshiaki Hayashi,[‡]

Yusuke Suganuma,[//] Hiroshi Nomura,[//] Osamu Fujita[†]

[†] Division of Mechanical and Space Engineering, Hokkaido University, Kita 13, Nishi 8, Kita-ku, Sapporo 060-8628, Japan

[‡] National Maritime Research Institute, 6-38-1 Shinkawa, Mitaka, Tokyo 181-0004, Japan

[§] JXTG Nippon Oil & Energy Corporation, 8 Chidoricho, Naka-ku, Yokohama, Kanagawa 231-0815, Japan

[//] College of Industrial Technology, Nihon University, 1-2-1 Izumi-cho, Narashino, Chiba 275-8575, Japan

KEYWORDS**:** Droplet evaporation; Low ignitability fuel; Cetane index; Low sulfur fuel; Marine fuel

ABSTRACT: The authors conducted droplet evaporation experiments of light cycle oil (LCO) at various ambient temperatures and pressures. Five kinds of LCO and three kinds of arranged-fuels were used. We investigated the evaporation characteristics of LCO and the relationships between the evaporation characteristics and the cetane index. In addition to that, a surrogate fuel composed of 4 chemical species, which can simulate the droplet evaporation characteristics of LCO, was suggested. Experimental results show that the differences in droplet lifetime between fuel species become larger with decreasing ambient temperature. This is because the low volatile component made the evaporation rate outstandingly slow at a low ambient temperature. Second, it was found that the relationship between droplet lifetime and the late-stage distillation temperature becomes stronger at low ambient temperature and high ambient pressure. By an analysis employing the properties of chemical species in LCO surrogate fuel, it is clarified that the mass evaporation rate becomes smaller than the internal diffusion, which is the condition similar to that in the distillation test. Finally, the relationship between the droplet lifetime and the cetane index was investigated. It can be concluded that the droplet lifetime is independent of the cetane index under all conditions tested in this study. The experimental data obtained by this research can be utilized for the validation of multi-component fuel droplet evaporation models in the future.

1. INTRODUCTION

Spray combustion is widely employed in industrial applications such as internal combustion engines, gas turbine engines, and rocket propulsion systems. However, the unstable combustion phenomena which cause a malfunction of the combustor has been reported.[1,2] For instance, knocking has been recognized as one of major problems for the reciprocating engine. An ignition delay of fuel is an important factor determining the occurrence of the knocking. To investigate the relationship between the ignition delay and the knocking, a study for single droplet ignition was conducted by some reserachers.[3] Furthermore, the ignition delay and combustion characteristics of biodiesel also have been studied because the practical usage of the next-generation fuel for an internal combustion engine is attempted in recent years.[4,5] Even though relationship between the combustion characteristics and the ignition delay has been investigated a lot, dominant factors for the ignition delay has not been clarified because the structure of spray combustion is much complicated, which is including atomization, droplet evaporation, and chemical reactions. Therefore, fundamental knowledge to clarify the dominant factors in the ignition delay is required. To clarify the complex mechanism of spray combustion, a numerical simulation tool has been strongly expanded. By employing the numerical simulation, not only the characteristics of spray[6] and spray flame such as jet flame[7,8] but also elements of spray flame such as atomization[9] and impingement[10] have been investigated. In particular, the prediction of fuel droplet size distributions and evaporation rate could affect the prediction of combustion properties including efficiency, stability, and pollutant formation rate. Noh *et. al.*[11] compared the spray combustion properties predicted by the different types of droplet evaporation models. As one of their findings, the predicted flame lift-off height depends on the droplet evaporation rate. It was revealed that the accuracy of a droplet evaporation model strongly influences the accuracy of the spray flame

structure predictions. Hence, the droplet evaporation model is one of the most important parts of the numerical simulation technology for the prediction of the spray combustion fields of the combustor. To develop the accurate droplet evaporation model, the experimental data for droplet evaporation is necessary for its validation. Nomura *et al.* investigated the droplet effect of ambient pressure on the evaporation characteristics of n-heptane[12] and n-hexadecane[13].

The droplet evaporation experimental data for market fuels have been also obtained by some researchers, while droplet combustion which is single droplet[14,15] as well as droplet cloud[16] have been studied a lot. For example, Elkotb *et al.*[17] studied the evaporation of commercial fuels (i.e., heavy diesel fuel, light diesel fuel, kerosene, gasoline, and their blends) at 400 °C and atmospheric pressure. Morin *et al.*[18] investigated the vaporization of vegetable oil droplets used as biofuels at high ambient temperature. Ghassemi *et al.*[19] investigated the vaporization of kerosene droplet at high temperatures and high pressures. Hashimoto *et al.*[20] investigated the evaporation characteristics of a palm methyl ester droplet at high ambient temperature. However, the experimental data of multi-component market fuel droplet evaporation are still very limited. For instance, the experimental data of droplet evaporation for light cycle oil (LCO) have not been obtained. The following is the reason why the experimental data of droplet evaporation for LCO is required.

As one of the significant environmental regulations, the International Maritime Organization (IMO) decided to tighten the global regulations of sulfur content in maritime fuel used on-board ships from 3.5% to 0.5% since 2020. To reduce the sulfur oxides in the exhaust gas, the fuel with low sulfur contents could lead to finding a solution to the root cause. Therefore, the efficient use of cracked middle distillates that contain fewer sulfur compositions is becoming important because of the increasing demand for diesel fuel.[21] As one of the cracked middle distillates, light cycle oil

(LCO) is a promising fuel of commercial diesel fuel, which is already mixed in maritime fuel as the fuel oil base material.[22] In response to the IMO regulations, some researchers investigated the fuel properties of LCO for practical usage and market growth.[23,24]. Hence, to correspond to the high market demand for LCO, the effect of using LCO on a combustor should be investigated.

Despite the advantages of LCO such as low sulfur compositions, LCO tend to contain a lot of aromatic compositions and be characterized as low ignitability fuel. Therefore, considering the increase of the situation that LCO is used as a part of a mixture product, the influence of using LCO on the diesel engines should be clarified. Xu *et al.*[25,26] investigated the combustion of LCO single droplets in normal and microgravity conditions. Imhof *et al.* [27] investigated emissions of LCO water-in-fuel emulsions with a test engine to reduce NO_x and unburned emission to follow IMO regulation. Tashima *et. al.*[28] demonstrated computational fluid dynamics (CFD) simulation including spray development and combustion process by using the fuel blending LCO. Furthermore, to develop the high precision simulation technique for LCO spray combustion, Takagi *et. al.*[29] developed a droplet evaporation model for multi-component fuel to investigate the relationships between evaporation characteristics and ignition delay. They numerically clarified that the effect of evaporation time on ignition delay become larger with increasing cetane index. Furthermore, they compared the predicted droplet evaporation characteristics of 13 kinds of LCO to clarify the relationship between the ignitability index and evaporation characteristics. However, the accuracy of the droplet evaporation model for LCO has not been clarified yet because the experimental data of LCO droplet evaporation have not been reported yet. To develop precise numerical simulation technologies for LCO spray combustion, the accuracy of the droplet evaporation model, which can affect the simulation results significantly, should be verified well by using experimental data.

In this study, the droplet evaporation characteristics of LCO at various ambient temperatures and pressures were investigated. The relationships between the evaporation characteristics and fuel ignitability index are investigated. The experimental data obtained by this study can be utilized for the future development of numerical simulation technology for LCO spray combustion as the validation data.

2. EXPERIMENTAL METHOD

2.1 LCO properties

This study used five kinds of LCO with different properties. Table 1 shows the properties of the LCO. L1, L2, L3, L12, and L13 are LCOs obtained at different oil refineries. L1, L2, L3 are the combination to investigate the effect of the differences of distillation characteristics. L12 L13 is the combination to have similar distillation characteristics. The fuels used in this study cover the hydrocarbon compositions of LCO not only before but also after hydrogenation.[30] As one of the remarkable characteristics of LCO, its cetane index is generally smaller than that of other transportation fuels, such as light oil and A-type heavy oil, which is why LCO is generally well known as a low-ignitibility fuel. The cetane index is applied instead of the cetane number when the cetane number cannot be obtained by the prescribed test engine. In this study, two kinds of cetane index are introduced. First on is the old cetane index (OCI) based on ASTM D976-66 or JIS K 2204:1983, which is expressed as follows:

$$\mathrm{OCI} = 0.49083 + 1.06577\mathrm{X} - 0.0010552\mathrm{X}^2 \tag{1}$$

$$\mathrm{X} = 97.833(\log_{10}(\mathrm{A}))^2 + 2.2088B_0 \log_{10}(A) + 0.0124\mathrm{B}_0^2 - 423.51\log_{10}(A) - 4.7808B_0 + 419.59 \tag{2}$$

$$\mathrm{A} = \frac{9}{5} T_{50} + 32 \tag{3}$$

where B_0 is the API gravity (-), and T_{50} is 50% volume distillation temperature (℃). Only 50% volume distillation temperature is considered in the OCI. Second one is the new cetane index (NCI) based on ISO 4264:2007 or JIS K 2280-5:2013, which is expressed as follows:

$$\begin{aligned}\mathrm{NCI} = {} & 45.2 + 0.0892(\mathrm{T}_{10} - 215) + (0.131 + 0.901B)(T_{50} - 260) \\ & + (0.0523 - 0.42B)(T_{90} - 310) + 0.00049\{(T_{10} - 215)^2 \\ & - (T_{90} - 310)^2\} + 107B + 60B^2\end{aligned} \tag{4}$$

$$\mathrm{B} = \exp\{-0.0035(1000\mathrm{D} - 850)\} - 1 \tag{5}$$

where T_{10} is the 10% volume distillation temperature (℃), T_{50} is the 50% volume distillation temperature (℃), T_{90} is the 90% volume distillation temperature (℃), and D is the density at 15 ℃ ($\mathrm{g/cm^3}$). In the NCI, 50%, 10%, and 90% volume distillation temperatures are considered, while only 50% volume distillation temperature is considered in the OCI. Note that in LCO, Takagi *et al.* [31] clarified that the ignition delay of LCO, which has the equivalent OCI to standard fuel of cetane number, can be related to that of the standard fuel of cetane number. However, the relationship between CI and evaporation characteristics has not been clarified.

As the other characteristics of LCO, a large number of aromatic hydrocarbons are contained in comparison with the other transportation fuels. Table1 shows that L1, L2, and L3 contains significant amounts of aromatic hydrocarbons. L1 and L3 contain over 80vol% aromatic hydrocarbons. In particular, L3 has over 20vol% aromatic hydrocarbons with at least three rings, which is the largest amount in the present LCO. L2 contains the largest amount of olefin in the

present LCO. L12 and L13 contain a large number of saturated hydrocarbons that are over 50vol%. Figure 1 shows the distillation curves of LCO and light oil [20]. According to Figure 1, L1 has the minimum difference between the initial boiling point (0%) and the ending point (100%) in LCO. On the other hands, L2 contains the largest number of the component with a low boiling point in LCO. Regarding the ending point of the distillation curve, L3 contains components with the highest boiling point. On the contrary, L12 and L13 have similar distillation characteristics. Note that the specific distillation temperatures in Figure 1 are printed in Supporting Information.

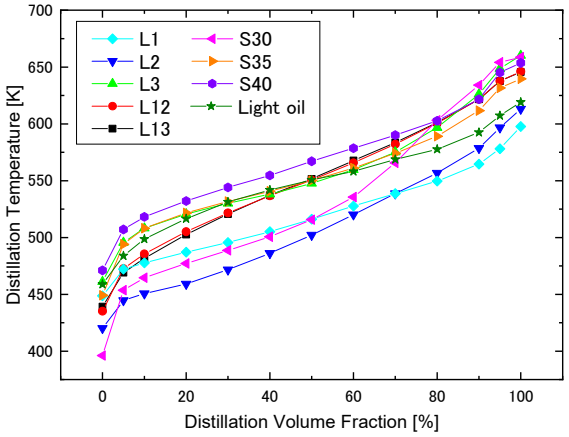

Figure 1. Distillation curves of LCO, arranged-fuels and light oil.

2.2 Arranged-fuels (S30, S35 and S40)

Arranged-fuels (S30, S35, and S40) were used to investigate the effect of the differences between the OCI and NCI on the evaporation characteristics of LCO. The arranged-fuels, are made to have almost the same NCI, are the liquid mixtures of refinery feedstocks and solvents. LCO used in this study has a variety of not only distillation characteristics but also cetane index. This makes it difficult to clarify whether the distillation characteristics or the cetane index have related to the evaporation characteristics. To clarify the relationship between the cetane index and droplet evaporation characteristics, the authors made the arranged-fuels, which has different distillation

characteristics but almost the same cetane index. The properties of the arranged-fuels are shown in Table 1.

Table 1. Properties of light cycle oil and arranged-fuel used in this study

			Light Cycle Oil					Arranged-Fuel		
			L1	L2	L3	L12	L13	S30	S35	S40
Density(15℃)		g/cm^3	0.9323	0.9266	0.9659	0.9018	0.8931	0.8834	0.8968	0.9028
Flash point		℃	68	52	N/A	N/A	67	29	79	82
Dynamic viscosity(30℃)		mm^2/s	2.169	2.097	N/A	N/A	3.425	2.454	3.844	4.582
Dynamic viscosity(50℃)		mm^2/s	1.522	1.493	2.469	2.295	2.256	1.724	2.497	2.898
Water content		wt%	0.00	0.00	N/A	N/A	0.00	0.00	0.00	0.00
Pour point		℃	<-45	<-45	N/A	N/A	-2.5	-30.0	-22.5	-22.5
CCAI		-	911	907	935	875	855	857	855	856
Old cetane index (JIS K 2204)		-	15	13.0	13.5	33.0	36.0	30.0	34.5	36.5
New cetane index (ISO 4264)		-	19.8	22.5	23.1	32.5	34.5	35.5	35.2	35.3
10%carbon residue		wt%	0.1	0.11	N/A	N/A	0.05	0.02	0.46	0.05
Sulfur		wt%	0.14	0.13	0.39	0.049	0.058	0.047	0.14	0.073
Nitrogen		wt%	0.011	0.012	N/A	N/A	0.016	0.008	0.04	0.024
Carbon		wt%	90.2	89.9	N/A	N/A	88.6	88.8	88.4	88.8
Hydrogen		wt%	9.6	9.9	N/A	N/A	11.3	11.1	11.4	11.1
Molecular structures	Saturated molecule	vol%	14.3	16.7	14.6	35.0	39.8	39.2	45.4	44.8
	Olefin	vol%	1.5	16.8	0.8	7.0	6.2	4.5	3.0	7.4
	Aromatics	vol%	84.2	66.5	84.6	58.0	54.0	56.3	51.6	47.8
	1ring aromatics	vol%	36.6	33.2	16.5	21.8	20.7	34.1	17.9	12.8
	2ring aromatics	vol%	43.6	27.8	47.4	24.6	22.8	17.9	23.9	18.5
	over 2 ring aromatics	vol%	4.0	5.5	20.7	11.6	10.5	4.3	9.8	16.5

2.3 Experimental setup and test conditions

Figure 2 shows the experimental setup [20] and the droplet suspend holder used in this study. The pressure vessel (inner diameter: 100 mm; inner height; 229 mm) was made by extra-super duralumin (JIS: A7075). The pressure vessel was filled with N_2 before the experiment to observe

a pure evaporation phenomenon without combustion. A charge-coupled device (CCD) video camera and a high-speed camera (DITECT, HAS-X) was used to observe the inside of the pressure vessel. The CCD video camera observed the droplet generating process. A fuel droplet with a diameter in the range of $0.5 \pm 15\%$ mm was suspended on the intersection point of two Al_2O_3/SiO_2 fibers with 7 μm diameter. The fuel was pumped with a microflow pump to the tip of the glass needle (outer diameter: 40 μm) of the droplet generator. After the fuel droplet was suspended at the intersection point of the droplet suspender, the glass needle was evacuated in preparation for the droplet insertion of the droplet into the hot chamber. A linear slider-crank mechanism was applied to the fuel droplet elevator to reduce the impact on the suspended droplet during the droplet insertion process. The traveling time of the droplet during the insertion into the hot chamber was 0.26 s, whose traveling distance is 6 mm. We compared the measured droplet diameter before and

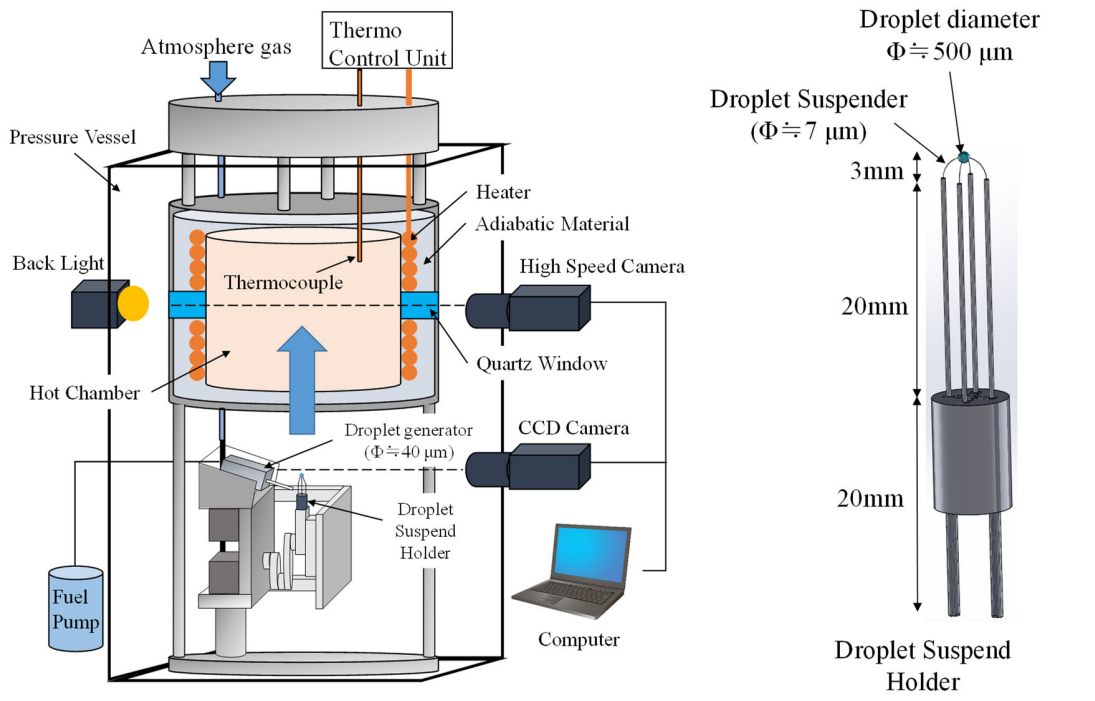

(a) Whole of experimental setup (b) Schematic of the droplet holder

Figure 2. Schematic of the experimental setup for the droplet evaporation experiment

after droplet insertion for all measured experimental data in the case of L1 to clarify the effect of the linear slider-crank mechanism on the evaporation characteristics. As a result, the average error of diameter difference is less than 5%. The ambient temperature (T_{amb}) inside the hot chamber was arbitrarily controlled in the range of 473-873 K by a thermal control unit. The images of an evaporating droplet were taken with a high-speed camera with backlit photography. The recorded backlit image of an evaporating fuel droplet was analyzed by using a self-made image analyzer program [32]. Figure 3 shows the details of the image analysis in this study. Each backlit image of a fuel droplet was divided into horizontal line sections with a vertical thickness of 2 pixels. The average horizontal intensity profiles were calculated for each section. The edge of a droplet was determined as the farthest position from the suspender at which the intensity was less than $(I_A + 2I_B)/3$, where I_A and I_B were the average intensities of the background and droplet, respectively. The droplet volume was calculated by an ellipsoidal approximation using the determined edge. Finally, the droplet diameter was defined as the diameter of a sphere with the same volume. The measurement limit of the droplet diameter using the image analyzer was under 0.078 mm, which corresponded to D^2/D_0^2 of 0.025.

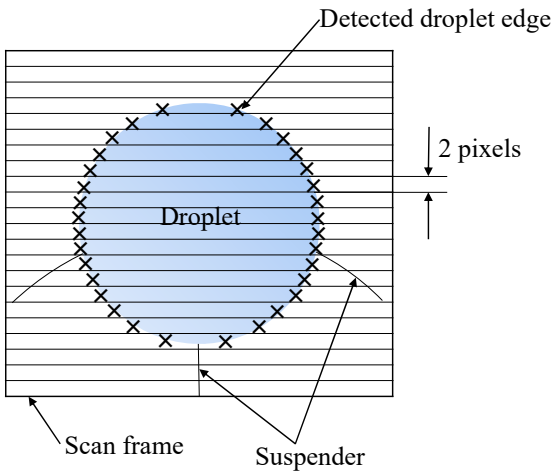

Figure 3. Schematic of the image analysis used to measure the droplet diameter

Figure 4 describes the definition of the periods during the droplet evaporation. The squared diameter was normalized by the squared initial diameter. Note that the droplet diameter when the fuel droplet was inserted in the hot chamber was defined as the initial droplet diameter in this study.

In the droplet evaporation experiments, the droplet diameter initially increases because of the thermal expansion effect caused by momentarily increasing the inner droplet temperature, which is shown as an initial heating period (τ_i/D_0^2). In the initial heating period, most of the heat energy from the ambient gas into the droplet is consumed to heat up the droplet. Therefore, decreasing the droplet density leads to an increase in the droplet diameter until the droplet evaporation rate becomes equal to the thermal expansion rate. The droplet diameter decreases monotonically after the droplet diameter reaches the maximum. As the indicator of the droplet lifetime, the 95vol% lifetime (τ_{95}/D_0^2) was defined as the period between the time when the fuel droplet was inserted into the hot chamber and the time when the droplet volume decreased to 5% of the initial volume equivalent to a relative diameter square of 13.6%. The droplet lifetime was also normalized by the second power of the initial droplet diameter because the initial droplet diameter strongly affects the droplet lifetime. The period obtained by removing the initial heating period from the 95vol% lifetime is defined as the main evaporation period (τ_{evap}/D_0^2).

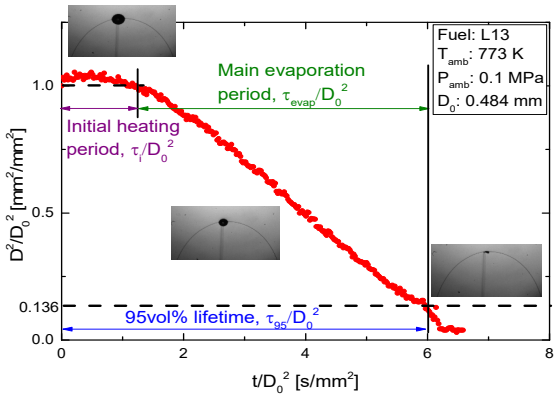

Figure 4. Definition of periods during the droplet evaporation

3. RESULTS AND DISCUSSIONS

3.1 Effect of the ambient temperature on the evaporation characteristics for LCO and arranged-fuels

Figure 5 shows the τ_{95}/D_0^2 of LCO in the ambient temperature range of 473-873 K at the ambient pressures (P_{amb}) of 0.1, 0.5, and 1.0 MPa. The differences of τ_{95}/D_0^2 between each LCO clearly become large with decreasing ambient temperature at all ambient pressures. In particular, at T_{amb} =473 K, L1 has the smallest τ_{95}/D_0^2 at all ambient pressures. Subsequently, τ_{95}/D_0^2 become large in the order of L2, L12, and L3. The reason for the pressure dependence of L13 becoming different from the other LCO at the lower ambient temperature will be discussed in Section 3.2. Figure 6 shows the τ_{95}/D_0^2 of the arranged-fuels in the ambient temperature range of 473-873 K at the ambient pressures of 0.1, 0.5, and 1.0 MPa. Similar to LCO, the trend that the differences of τ_{95}/D_0^2 become

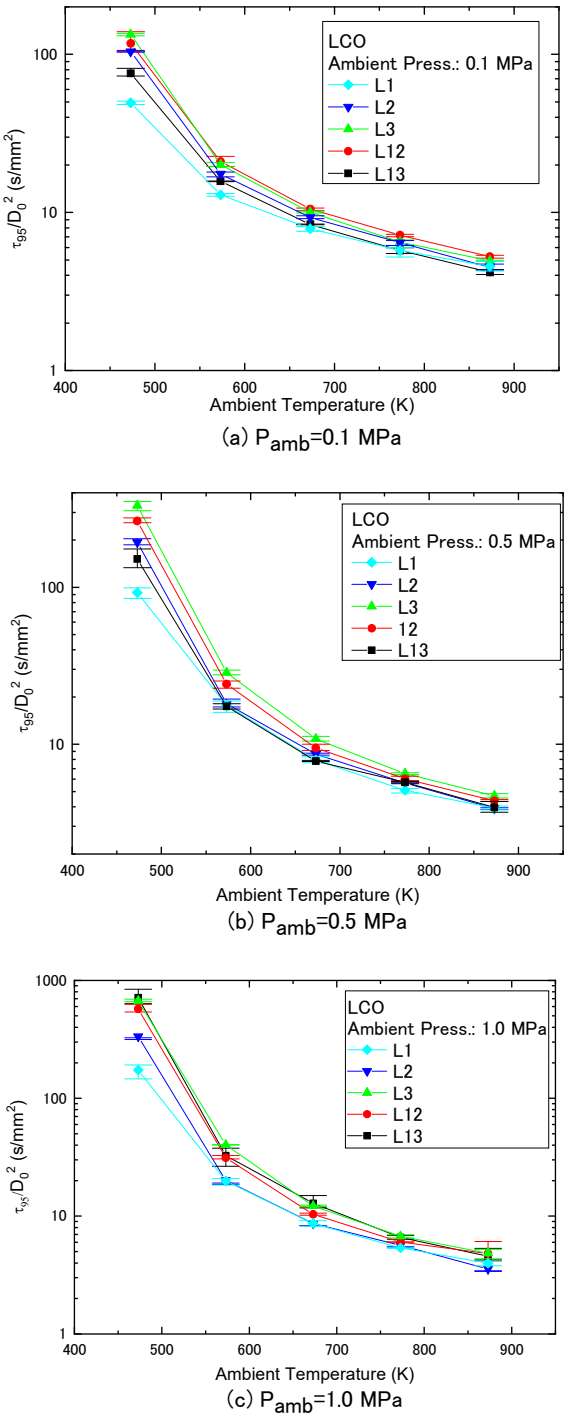

Figure 5. Normalized 95vol% lifetime (τ_{95}/D_0^2) as a function of the ambient temperature for LCO

large with decreasing ambient temperature can be seen at all ambient pressures. On the other hands, the differences of τ_{95}/D_0^2 between S30 and S40 become much small at various ambient temperatures, except 473 K, at all ambient pressures.

The reason that the differences of τ_{95}/D_0^2 between the fuels become large at the low ambient temperature will be discussed in the parts that follow. Figure 7 shows the histories of the D^2/D_0^2 of LCO and the arranged-fuels at various ambient temperatures and P_{amb} = 0.1 MPa. Note that the detailed law data for all histories of the D^2/D_0^2 obtained in this study are provided in the Supporting Information section of this paper. These D^2/D_0^2 history data will be directly used for the future validation for the multi-component droplet evaporation model development. In particular, the sensitivity of the components in fuel for the models can be validated in detail, because the D^2/D_0^2 histories significantly differ each other when the components are different as

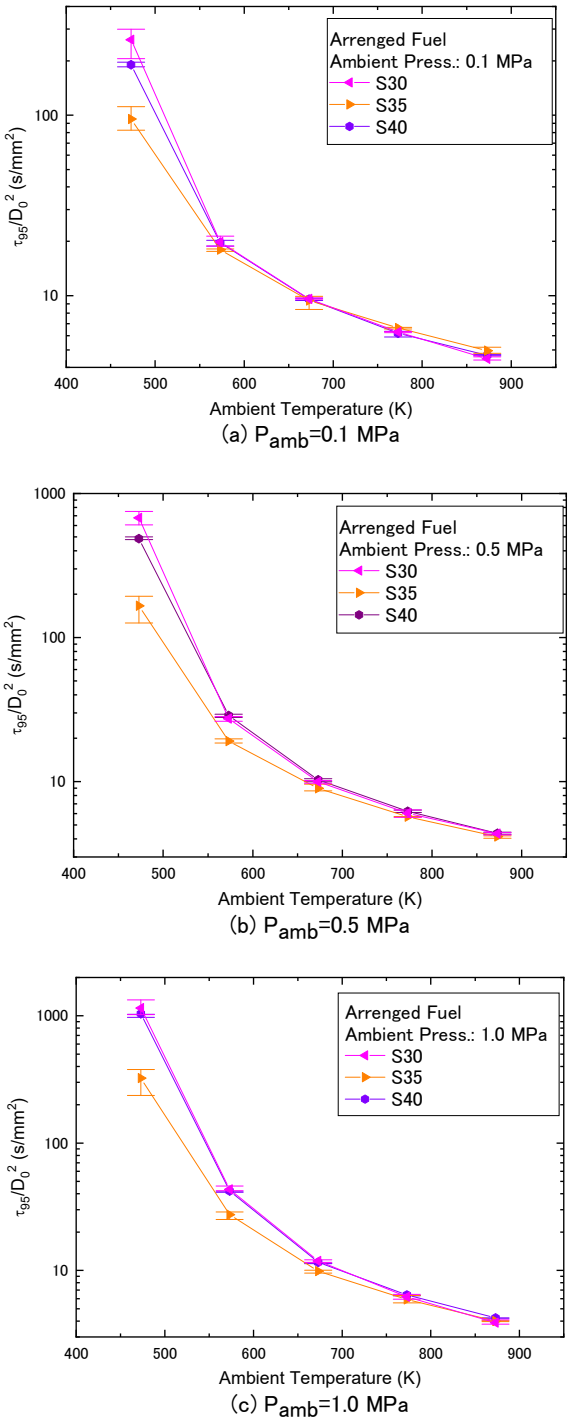

Figure 6. Normalized 95vol% lifetime (τ_{95}/D_0^2) as a function of the ambient temperature for the arranged-fuel

observed in Figure 7 (a). According to Figure 7-(a), the rate of decrease in D^2/D_0^2 become obviously slow as time goes by. The rate of decrease in D^2/D_0^2 approaches to a constant rate during τ_{evap}/D_0^2 with increasing ambient temperature (Figure 7). To evaluate the rate of decrease in D^2/D_0^2, this study defined the instantaneous evaporation coefficient (K_{inst}) to quantitively evaluate the rate of decrease in D^2/D_0^2 . K_{inst} was calculated by the following procedures: first, the original data plots during τ_{evap}/D_0^2 consisting of 200-3000 plots were thinned to 40-50 plots. Second, the smoothing differentiation method, called as the SG method [33], was applied to the thinned data plots. The absolute value of the differential coefficient calculated by the SG method gave K_{inst}. Figure 8 shows the K_{inst} of LCO and the arranged-fuels in various ambient temperatures at P_{amb} = 0.1 MPa. The fluctuation of K_{inst} history shown in Figure

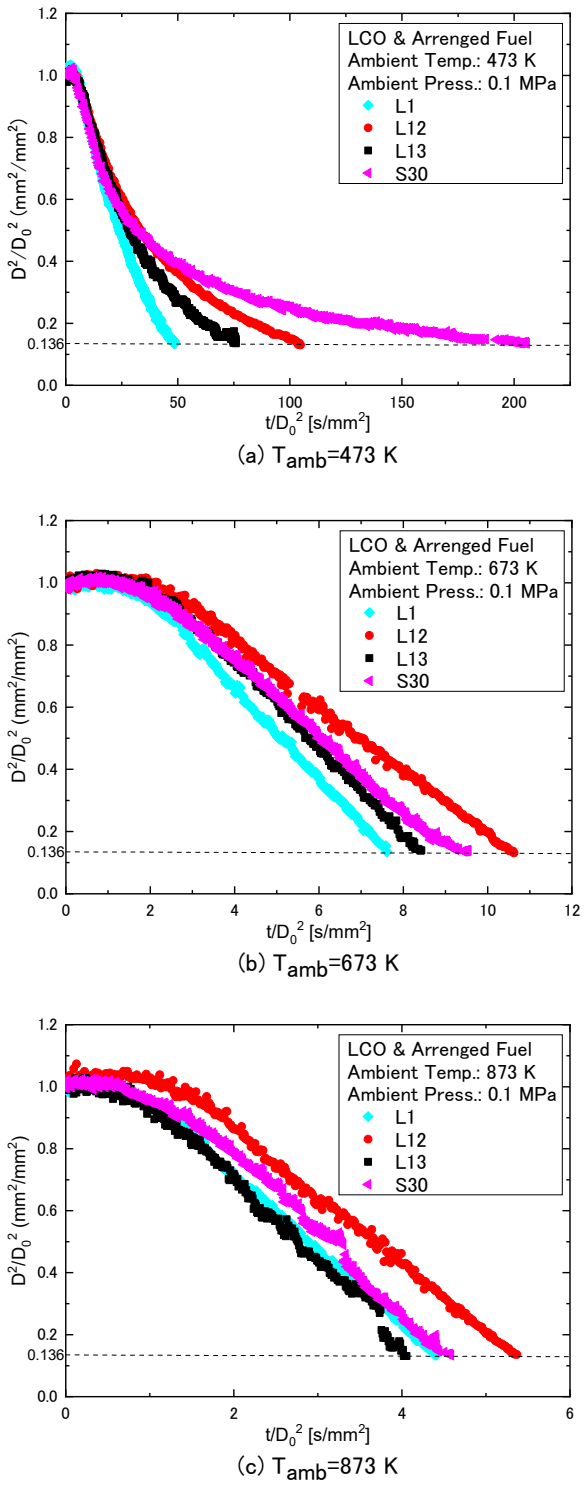

Figure 7. Examples of the histories of normalized D^2 for LCO

8 is caused by image analysis error. A decreasing of K_{inst} indicates that the rate of decrease in D^2/D_0^2 shown in Figure 7 is not constant as time goes by at T_{amb}=473 K. The gradient shown in Figure 8-(a) become steep in the order of S30, L12, L13, and L1. This order matches the order of the highest boiling point component in the fuel. Hence, it is considered that the end point of distillation curve may make the rate of decrease in D^2/D_0^2 slower even though LCO contain the various chemical species having the various boiling point. Note that there is an obvious difference of K_{inst} between L12 and L13 even though the difference of the highest boiling point component between L12 and L13 is much small. To clarify this reason, much fundamental experimental data based on the single component are necessary. However, Figure 8-(b) and (c) shows that the difference of K_{inst} between the fuels decrease, and the absolute value of K_{inst} reaches an almost constant value with

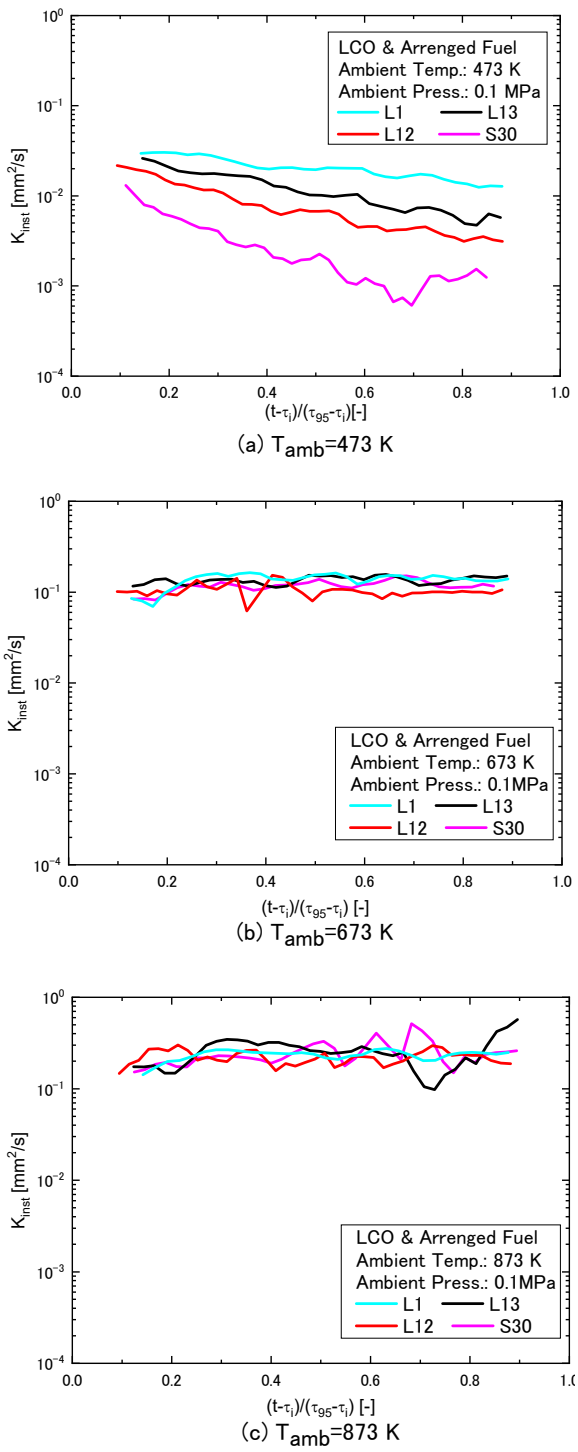

Figure 8. Instantaneous evaporation coefficient (K_{inst}) for LCO and the arranged-fuels

increasing ambient temperature. These findings confirm that the rate of decrease in D^2/D_0^2 is almost constant at the higher ambient temperature. On the other hand, the ambient pressure dependence on the evaporation characteristics will be discussed in section 3.3.

Table 2. Compositions and properties of L1 surrogate fuel

Molecular Formula		$C_{10}H_{14}$	$C_{11}H_{10}$	$C_{16}H_{34}$	$C_{20}H_{42}$
Molecular Weight	g/mol	134	142	226	282
Mass Fraction	-	0.3116	0.4402	0.1753	0.0729
Boiling Point	°C	169.1	244.6	286.9	344.1
Density (15°C)	g/cm^3	0.8708	1.027	0.7773	0.7908

3.2 Development and validation of the surrogate fuel for LCO

In the numerical simulation, a surrogate fuel is usually used. A surrogate fuel consists of distinct fuel to simulate a certain characteristic of physical phenomena. By using a surrogate fuel in combustion simulation, we are able to utilize the detailed chemical reaction mechanism. However, the surrogate fuel of LCO has not been developed. To conduct the precise combustion simulation using LCO in future works, the surrogate fuel of LCO should be developed.

To simulate the evaporation characteristics of LCO (L1), we choose the chemical species and determine their fractions so that the distillation characteristics of LCO can be reproduced by the surrogate fuel. Table 2 shows the compositions and properties of the developed surrogate fuel. LCO surrogate fuel, which is treated as a mixture composed of tert-butylbenzene ($C_{10}H_{14}$), 1-methylnaphthalene ($C_{11}H_{10}$), n-hexadecane ($C_{16}H_{34}$) and n-eicosane ($C_{20}H_{42}$) with mass fraction of 0.3116, 0.4402, 0.1753, and 0.0729, respectively, was developed. The boiling point with volume

Table 3. Properties of L1 surrogate fuel

Fuel		L1	Surrogate Fuel
Density (15°C)	g/cm^3	0.9323	0.9173
Cetane Index [JIS K 2280]		19.8	19.7
Sulfur	wt%	0.14	0
Nitrogen	wt%	0.011	0
Carbon	wt%	90.3	89.9
Hydrogen	wt%	9.6	10.1
C/H ratio	-	9.4	8.9
Saturated molecule	vol%	14.3	16
Olefin	vol%	1.5	0
Aromatics	vol%	84.2	84
1ring aromatics	vol%	36.6	36
2ring aromatics	vol%	43.6	48
over 2 ring aromatics	vol%	4	0

fraction for each chemical species was compared with the distillation curve of L1. The boiling temperature width of the surrogate fuel stays within the boiling temperature range of LCO, especially the first drop point and ending point of L1 distillation curve is in good agreement with the boiling point of components in the surrogate fuel. Second, the properties of the surrogate fuel are compared with that of LCO. According to table 3, the surrogate fuel emulates the density at 15 ℃, the NCI calculated by eq 4, the C/H ratio, and the molecular types of L1. Hence, the thermodynamic properties and the ratio of molecular structure types of the surrogate fuel

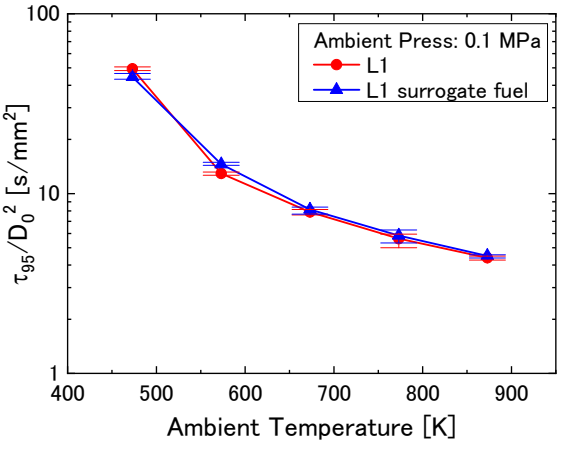

Figure 9. Validation of LCO surrogate fuel at various ambient temperature.

are in good agreement with those of L1. Finally, the droplet evaporation experiments of the surrogate fuel were conducted in the present set-up to validate the evaporation characteristics. Figure 9 shows the comparison of droplet lifetimes between the surrogate fuel and L1 at various ambient temperatures. It is found that the droplet lifetimes of the surrogate fuel are in good agreement with that of L1 at various ambient temperatures. Especially, the difference of droplet lifetime between L1 and the surrogate fuel was less than 5% in higher ambient temperature. It can be concluded that we succeeded to develop the LCO surrogate fuel, which well simulates the droplet evaporation characteristics of LCO.

3.3 Effect of the ambient pressure on the evaporation characteristics for LCO and arranged-fuels.

Figure 10 shows the pressure dependence of τ_{95}/D_0^2 for L1, L2, and L13 at T_{amb} = 473 and 873 K. When $T_{amb} = 873\ K$, the difference of τ_{95}/D_0^2 between the fuels become smaller at all ambient pressure. On the other hands, when $T_{amb} = 473$ K, the difference of τ_{95}/D_0^2 between the fuels become large at all ambient pressures. Accordingly, the τ_{95}/D_0^2 of L13 is larger than that of L1 and smaller than that of L2 at $T_{amb} = 473$ K and P_{amb}= 0.1 MPa. However, the τ_{95}/D_0^2 of L13 steeply increase with increasing ambient pressure (Figure 10). Eventually, the τ_{95}/D_0^2 of L13 becomes the largest among LCO at

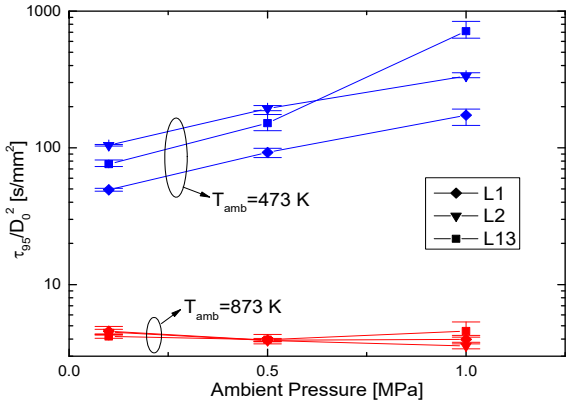

Figure 10. Normalized 95vol% lifetime (τ_{95}/D_0^2) as a function of the ambient pressure for LCO

P_{amb}= 1.0 MPa. Figure 10 depicts the τ_{95}/D_0^2 become large in the order of increasing the ending point of the distillation curve shown in Figure 1.

Figure 11 shows the relationships between the distillation temperature and τ_{95}/D_0^2 at various ambient temperature at P_{amb}= 0.1 and 1.0 MPa. In both figures (Figure 11), the left region shows the range of 10vol% distillation temperature for all species, whereas the right region illustrates the range of 90vol% distillation temperature for all species. The scattering of τ_{95}/D_0^2 is smaller at the high ambient temperature at various ambient pressures. In other words, the droplet lifetimes are independent of the distillation temperatures at the high ambient temperature at various ambient pressures. However, τ_{95}/D_0^2 become longer with increasing 90vol% distillation temperatures in low ambient temperatures. In Figure 11, linear least-squares fitting equations for T_{amb}= 473 K are shown. Apparently, the gradient of the fitting line becomes steeper in higher ambient pressure. This means that the relationships between 90vol% distillation temperature and droplet lifetime become strong in low

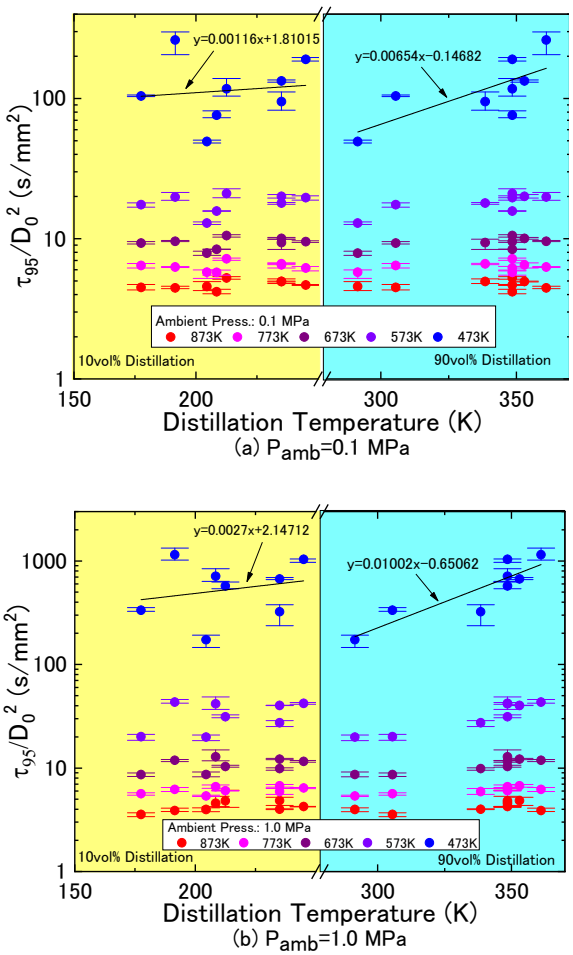

Figure 11. Normalized 95vol% lifetime (τ_{95}/D_0^2) as a function of the distillation temperature for the fuels used in this study

ambient temperature and high ambient pressure. The reason for this relationship will be discussed in the paragraphs that follow.

We conducted a Peclet number analysis to discuss the above relationship. According to ref. [34], the molar weight variation has a decisive influence on the ratio of the characteristics time scales of the droplet lifetime and the mass diffusion. The gasification Peclet number [35] shown in eq 6 can assess the relative dominance of the diffusion limit versus distillation behavior.

$$Pe = \frac{\dot{m}_{vap}}{2\pi D_d \Gamma_l \rho_l} \tag{6}$$

where Pe is the Peclet number $(-)$, $\dot{m}_{vap}$ is the mass evaporation rate (kg/s), D_d is the droplet diameter (m), Γ_l is the diffusion coefficient inside the droplet ($\mathrm{m^2/s}$), and ρ_l is the droplet density ($\mathrm{kg/m^3}$). However, the Peclet number given by eq 6 is not considering the multi-component interaction effect. Therefore, the Peclet number on droplet evaporation was estimated in this paper by rearranging eq 6 to multi-component fuel.

The Peclet number shown in eq 6 can be rearranged by using the Spalding model [34]. Mass evaporation rate ($\dot{m}_{vap}$) and evaporation constant (K) is described as the following.

$$\dot{m}_{vap} = \frac{4\pi k_g r_s}{c_{p,g}} \ln\left(B_q + 1\right) \tag{7}$$

$$K = \frac{8k_g}{\rho_l c_{p,g}} \ln\left(B_q + 1\right) \tag{8}$$

Where k_g is the thermal conductivity of ambient gas (W/m-K), $c_{p,g}$ is the specific heat of gas (J/kg-K), r_s is droplet radius (m), ρ_l is fuel density (kg/ m^3), B_q is Spalding number (-). Substituting eq 8 into eq 7, the mass evaporation rate can be expressed as a function of evaporation constant (K), and the Peclet number shown in eq 6 can be rearranged as the following.

$$Pe = \frac{\dot{m}_{vap}}{2\pi D_d \Gamma_l \rho_l} = \frac{1}{4\pi r_s \Gamma_l \rho_l} \frac{\pi r_s \rho_l}{2} K = \frac{K}{8\Gamma_l} \quad (9)$$

Note that the surrogate fuel developed in section 3.2 was used to calculate the diffusion coefficient inside the droplet (Γ_l). In, our analysis, K was replaced by instantaneous evaporation coefficient, K_{inst}, which was obtained from experimental results shown in Figure 8.

Figure 12 shows the history of estimated Peclet number at two ambient conditions, (1) $T_{amb} =$ 473 K and $P_{amb} = 1.0$ MPa (2) $T_{amb} = 873$ K and $P_{amb} = 0.1$ MPa. *Pe* shown in Figure 12 are calculated by eq 9. Furthermore, K_{inst} used in eq 9 was obtained from experimental results. This is why *Pe* shown in Figure 12 is renewed moment by moment. Note that the diffusion coefficient inside the droplet (Γ_l) is a function of droplet temperature (Appendix). As a droplet temperature, 473 K which is the same temperature with ambient temperature was applied in case (1), and 617 K which is the same temperature with the boiling point of n-eicosane was applied in case (2). According to Figure 12, the Peclet number in case (1) decreases as time goes by although the Peclet number in case (2) shows almost constant value, and the Peclet number in case (1) becomes much smaller than that in case (2). When the Peclet number becomes larger, the internal diffusion is not able to catch up with the mass evaporation rate. Therefore, the droplet composition remains unchanged [34], thus indicating that evaporation characteristics approach the evaporation characteristics of the single component described by the D^2 law. This is why the correlation

between the droplet evaporation characteristics and the distillation process is weak at high ambient temperatures. On the other hand, when the Peclet number becomes smaller, the mass evaporation rate becomes sufficiently slow compared with the internal diffusion. This result implies that the relationship between the droplet evaporation characteristics and the distillation curve is strong. This is why the D^2 law cannot be applied to the evaporation of multi-component fuel droplet at the low ambient temperature. Moreover, the evaporation rate is further reduced at high pressure ambient. Therefore, the tendency of droplet lifetime lengthening with increasing the ending point of the fuel distillation temperature become strong under the low ambient temperature and high ambient pressure.

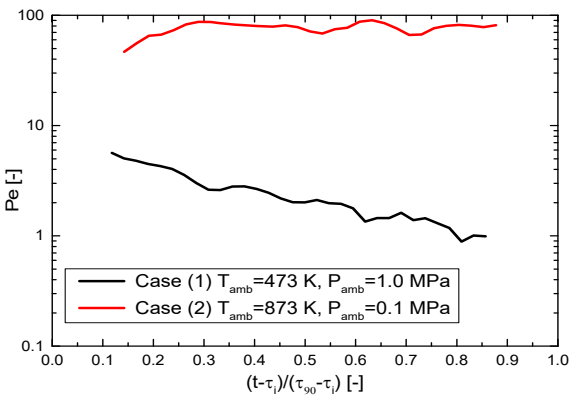

Figure 12. Histories of estimated Peclet number during main evaporation term

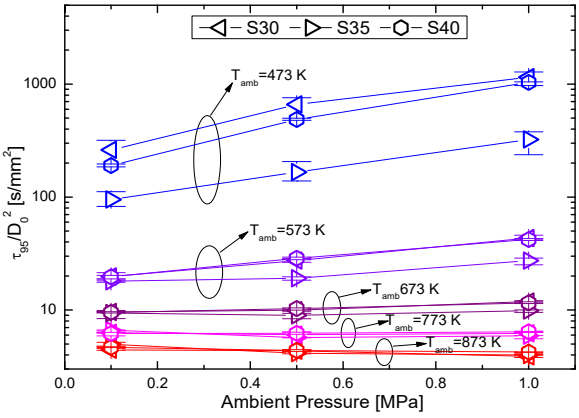

Figure 13. Normalized 95vol% lifetime (τ_{95}/D_0^2) as a function of the ambient pressure for the arranged-fuels

The relationships between the different ways of calculating the cetane index and droplet evaporation characteristics were investigated. Figure 13 shows the pressure dependence of τ_{95}/D_0^2

for the arranged-fuels. As mentioned in Section 2.2, the arranged-fuels were made such that their NCI is 35. Figure 13 shows that the difference of τ_{95}/D_0^2 between the fuels became small at $T_{amb} = 673, 773,$ and 873 K. However, the difference of τ_{95}/D_0^2 between the fuels became large at $T_{amb} =$ 473 and 573 K. As discussed in Section 3.1, this behavior is caused by components with a high boiling point, which make the rate of decrease in D^2/D_0^2 slower. By contrast, the OCI of S30, S35, and S40 are increased in the order of S30, S35, and S40. However, the τ_{95}/D_0^2 of S30, S35, and S40 is increased in the order of S30, S40, and S35. These results implied that the τ_{95}/D_0^2 is independent of the OCI. Simultaneously, the τ_{95}/D_0^2 of S30, S35, and S40 increased in the order of S30, S40, and S35, although all the arranged-fuels have the almost same new cetane index that is 35. In conclusion, τ_{95}/D_0^2 cannot be associated with the cetane index when the cetane index is 35.

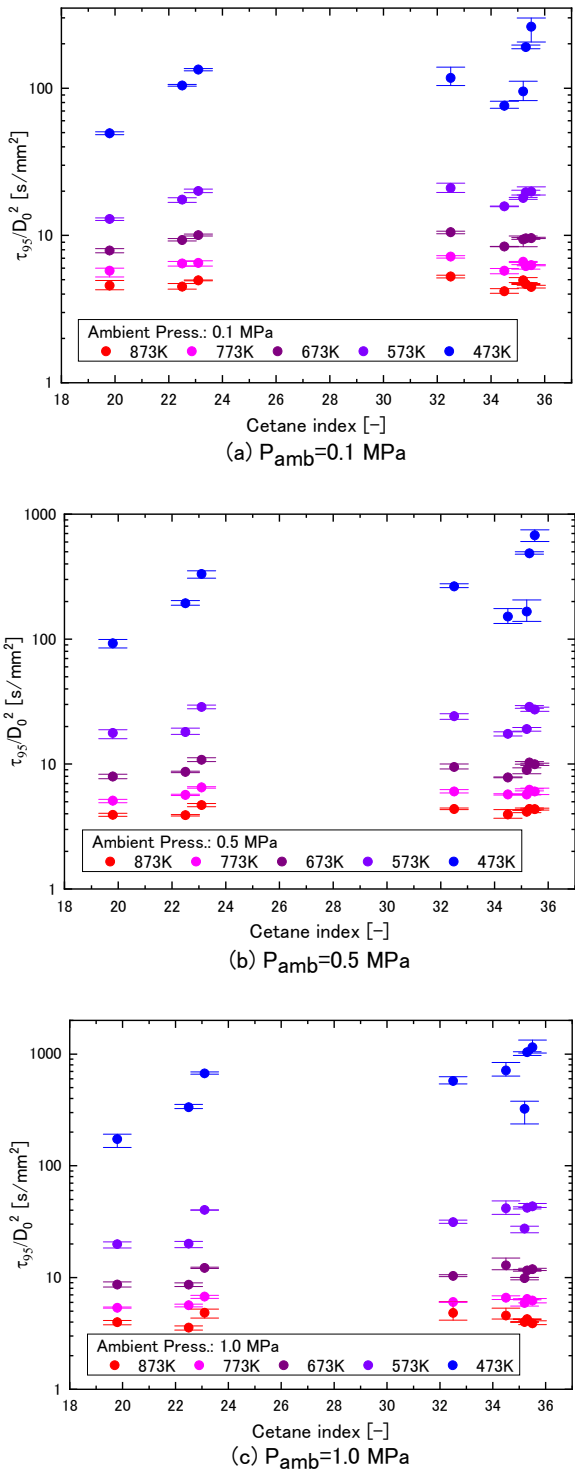

Figure 14. Normalized 95vol% lifetime (τ_{95}/D_0^2) as a function of the cetane index for the fuels used in this study

474 Finally, the relationships between the droplet lifetime and the cetane index were investigated.
475 Figure 14 shows the relationships between the cetane index calculated by eq 4 and τ_{95}/D_0^2 at the
476 various ambient pressures (0.1, 0.5, and 1.0 MPa) and temperatures. It was found that there is no
477 correlation between the cetane index and τ_{95}/D_0^2. It can be concluded that the droplet lifetime is
478 independent of the cetane index introduced in this paper under the conditions tested. Furthermore,
479 the correction coefficient between the droplet evaporation lifetime and the mole fraction of mono-,
480 di-, and 3+ cyclic aromatic compounds at all experimental conditions were investigated. However,
481 we found that there is little correlation between the evaporation characteristics and aromatic
482 compositions. In actuality, fuel droplets will continuously evaporate at higher temperature and
483 pressure conditions after the ignition. Therefore, the clarification of droplet evaporation
484 characteristics in such conditions is also necessary as the future research.
485
486 4. CONCLUSIONS
487 In this study, LCO single droplet evaporation experiments were conducted at various ambient
488 temperature and pressure to obtain the validation data. The detailed droplet evaporation history
489 data of fuels with various composition ratios were obtained by this study. The data can be utilized
490 for the validation of the sensitivity of the components for multi-component droplet evaporation
491 models in the future. In addition, development and validation of the surrogate fuel for LCO (L1)
492 were conducted. Finally, the relationships between the evaporation characteristics and cetane index,
493 which is one of the indicators for fuel ignitability, were investigated. The main findings are as
494 follows:
495 1. The droplet lifetime decreases with increasing ambient temperature for all fuel species. The
496 differences of droplet lifetime between the fuels become larger with decreasing ambient

497 temperature. This is because the low volatile component made the evaporation rate
498 outstandingly slow at low ambient temperature.
499 2. The evaporation characteristics of the surrogate fuel are in good agreement with that of LCO
500 at various ambient temperatures. Especially, the difference of droplet lifetime between L1 and
501 the surrogate fuel is less than 5% in higher ambient temperature.
502 3. The droplet evaporation lifetime can be characterized by the late stage distillation temperature
503 at a low ambient temperature. The correlation between the droplet lifetime and the late-stage
504 distillation temperature becomes stronger with increasing ambient pressure because the mass
505 evaporation rate becomes smaller than the internal diffusion, which is a condition similar to
506 that in the distillation test. Hence, the tendency of the droplet lifetime to increase with
507 increasing the end point of the fuel distillation temperature become strong at low ambient
508 temperature and high ambient pressure.
509 4. The droplet lifetime of LCO and the arranged-fuels is independent of the cetane index under
510 experimental conditions shown in this paper.
511

512 Appendix Diffusion coefficient inside a droplet

513 The diffusion coefficients used in the Peclet number were estimated as the following. First, the
514 binary diffusion coefficient can be calculated from ref. [36] as

515

516 $$D_{i,j} = 8.93 \times 10^{-8} \frac{V_j^{0.267}}{V_i^{0.433}} \frac{T}{\eta_j}$$

517

where $D_{i,j}$ is the binary diffusion coefficient of species i and j in the droplet; V is the molar volume of species i; T is droplet temperature; η_j Pearson's the viscosity of species i. For multi-component fuels, the mixture of all the species except i is assumed as the second species m. Then, the diffusion coefficient of species i for the mixture can be described as

$$D_{i,m}\eta_m^{0.8} = \sum_{\substack{j=1 \\ j\neq i}}^{N_l} x_j D_{i,j}\eta_j^{0.8}$$

where x_j is the mole fraction of species j and N_l is the number of species. Hence, the binary diffusion coefficient (Γ_l) used for Peclet number in eq 9 can be averaged as the following.

$$\Gamma_l = \sum_{i=1}^{N_l} x_i D_{i,m}$$

■ ASSOCIATED CONTENT

Supporting Information.

The following files are available free of charge.

Experimental data_LCO (xlsx)

■ AUTHOR INFORMATION

Corresponding Author

* Email: nozomu.hashimoto@eng.hokudai.ac.jp

Notes

The authors declare no competing financial interest.

■ REFERENCES

(1) Poinsot, T. Prediction and Control of Combustion Instabilities in Real Engines. *Proc. Combust. Inst.* **2017**, *36* (1), 1–28. https://doi.org/10.1016/j.proci.2016.05.007.

(2) Terashima, H.; Matsugi, A.; Koshi, M. End-Gas Autoignition Behaviors under Pressure Wave Disturbance. *Combust. Flame* **2019**, *203*, 204–216. https://doi.org/10.1016/j.combustflame.2019.02.011.

(3) Burkert, A.; Paa, W. Ignition Delay Times of Single Kerosene Droplets Based on Formaldehyde LIF Detection. *Fuel* **2016**, *167*. https://doi.org/10.1016/j.fuel.2015.11.051.

(4) Bittle, J. A.; Knight, B. M.; Jacobs, T. J. Interesting Behavior of Biodiesel Ignition Delay and Combustion Duration. *Energy and Fuels* **2010**, *24* (8), 4166–4177. https://doi.org/10.1021/ef1004539.

(5) Shahabuddin, M.; Liaquat, A. M.; Masjuki, H. H.; Kalam, M. A.; Mofijur, M. Ignition Delay, Combustion and Emission Characteristics of Diesel Engine Fueled with Biodiesel. *Renew. Sustain. Energy Rev.* **2013**, *21*, 623–632. https://doi.org/10.1016/j.rser.2013.01.019.

(6) Kobashi, Y.; Zama, Y.; Kuboyama, T. Modeling Wall Film Formation and Vaporization of a Gasoline Surrogate Fuel. *Int. J. Heat Mass Transf.* **2020**, *147*, 119035. https://doi.org/10.1016/j.ijheatmasstransfer.2019.119035.

(7) Moriai, H.; Kurose, R.; Watanabe, H.; Yano, Y.; Akamatsu, F.; Komori, S. Large-Eddy Simulation of Turbulent Spray Combustion in a Subscale Aircraft Jet Engine Combustor—Predictions of NO and Soot Concentrations. *J. Eng. Gas Turbines Power* **2013**, *135* (9), 091503. https://doi.org/10.1115/1.4024868.

(8) Yu, P.; Watanabe, H.; Zhang, W.; Kurose, R.; Kitagawa, T. Flamelet Model for a Three-Feed Non-Premixed Combustion System with a Diluent Stream: Analysis and Validation of Quasi-Two-Dimensional Flamelet (Q2DF) Models. *Energy and Fuels* **2019**, *33* (5), 4640–4650. https://doi.org/10.1021/acs.energyfuels.9b00764.

(9) Tanimoto, D.; Shinjo, J. Numerical Simulation of Secondary Atomization of an Emulsion Fuel Droplet Due to Puffing: Dynamics of Wall Interaction of a Sessile Droplet and Comparison with a Free Droplet. *Fuel* **2019**, *252* (March), 475–487. https://doi.org/10.1016/j.fuel.2019.04.136.

(10) Zhang, Z.; Zhang, P. Cross-Impingement and Combustion of Sprays in High-Pressure Chamber and Opposed-Piston Compression Ignition Engine. *Appl. Therm. Eng.* **2018**, *144* (July), 137–146. https://doi.org/10.1016/j.applthermaleng.2018.08.038.

(11) Noh, D.; Gallot-Lavallée, S.; Jones, W. P.; Navarro-Martinez, S. Comparison of Droplet Evaporation Models for a Turbulent, Non-Swirling Jet Flame with a Polydisperse Droplet Distribution. *Combust. Flame* **2018**, *194*, 135–151. https://doi.org/10.1016/j.combustflame.2018.04.018.

(12) Nomura, H.; Ujiie, Y.; Rath, H. J.; Sato, J.; Kono, M. Experimental Study on High-Pressure Droplet Evaporation Using Microgravity Conditions. *Symp. Combust.* **1996**, *26* (1), 1267–1273. https://doi.org/10.1016/S0082-0784(96)80344-4.

(13) Nomura, H.; Murakoshi, T.; Suganuma, Y.; Ujiie, Y.; Hashimoto, N.; Nishida, H. Microgravity Experiments of Fuel Droplet Evaporation in Sub- and Supercritical Environments. *Proc. Combust. Inst.* **2017**, *36* (2). https://doi.org/10.1016/j.proci.2016.08.046.

(14) Xu, Y.; Avedisian, C. T. Combustion of N-Butanol, Gasoline, and n-Butanol/Gasoline Mixture Droplets. *Energy and Fuels* **2015**, *29* (5), 3467–3475. https://doi.org/10.1021/acs.energyfuels.5b00158.

(15) Jiang, L.; Elbaz, A. M.; Guida, P.; Al-Noman, S. M.; Alghamdi, I. A.; Saxena, S.; Roberts, W. L. Cenosphere Formation during Single-Droplet Combustion of Heavy Fuel Oil. *Energy and Fuels* **2019**, *33* (2), 1570–1581. https://doi.org/10.1021/acs.energyfuels.8b03632.

(16) Yoshida, Y.; Iwai, K.; Nagata, K.; Seo, T.; Mikami, M.; Moriue, O.; Sakashita, T.; Kikuchi, M.; Suzuki, T.; Nokura, M. Flame-Spread Limit from Interactive Burning Droplets in Microgravity. *Proc. Combust. Inst.* **2019**, *37* (3), 3409–3416. https://doi.org/10.1016/j.proci.2018.07.106.

(17) Elkotb, M. M.; Aly, S. L.; Elsalmawy, H. A. Evaporation Characteristics of Fuel and Multifuel Droplets. *Combust. Flame* **1991**, *85* (3–4), 300–308. https://doi.org/10.1016/0010-2180(91)90135-X.

(18) Morin, C.; Chauveau, C.; Gökalp, I. Droplet Vaporisation Characteristics of Vegetable Oil Derived Biofuels at High Temperatures. *Exp. Therm. Fluid Sci.* **2000**, *21* (1–3), 41–50. https://doi.org/10.1016/S0894-1777(99)00052-7.

(19) Ghassemi, H.; Baek, S. W.; Khan, Q. S. Experimental Study on Evaporation of Kerosene Droplets at Elevated Pressures and Temperatures. *Combust. Sci. Technol.* **2006**, *178* (9), 1669–1684. https://doi.org/10.1080/00102200600582392.

(20) Hashimoto, N.; Nomura, H.; Suzuki, M.; Matsumoto, T.; Nishida, H.; Ozawa, Y. Evaporation Characteristics of a Palm Methyl Ester Droplet at High Ambient Temperatures. *Fuel* **2015**, *143*, 202–210. https://doi.org/10.1016/j.fuel.2014.11.057.

(21) Muíková, Z.; Procháska, F.; Pospíil, M. Storage Stability of FCC Light Cycle Oil. *Fuel* **2010**, *89* (11), 3534–3539. https://doi.org/10.1016/j.fuel.2010.06.019.

(22) Kondrasheva, N. K.; Rudko, V. A.; Kondrashev, D. O.; Gabdulkhakov, R. R.; Derkunskii, I. O.; Konoplin, R. R. Effect of Delayed Coking Pressure on the Yield and Quality of Middle and Heavy Distillates Used as Components of Environmentally Friendly Marine Fuels. *Energy and Fuels* **2019**, *33* (1), 636–644. https://doi.org/10.1021/acs.energyfuels.8b03756.

(23) Jin, N.; Wang, G.; Yao, L.; Hu, M.; Gao, J. Synergistic Process for FCC Light Cycle Oil Efficient Conversion to Produce High-Octane Number Gasoline. *Ind. Eng. Chem. Res.* **2016**, *55* (17), 5108–5115. https://doi.org/10.1021/acs.iecr.6b00360.

(24) Pujro, R.; Falco, M.; Sedran, U. Production of Aromatic Compounds in the Heavy Naphtha and Light Cycle Oil Ranges: Catalytic Cracking of Aromatics and

620 C10naphthenic-Aromatics. *J. Chem. Technol. Biotechnol.* **2016**, *91* (2), 336–345.
621 https://doi.org/10.1002/jctb.4570.

622 (25) Xu, G.; Ikegami, M.; Honma, S.; Ikeda, K.; Nagaishi, H.; Dietrich, D. L.; Takeshita, Y.
623 Burning Droplets Composed of Light Cycle Oil and Diesel Light Oil. *Energy and Fuels*
624 **2002**, *16* (2), 366–378. https://doi.org/10.1021/ef010112r.

625 (26) Xu, G.; Ikegami, M.; Honma, S.; Sasaki, M.; Ikeda, K.; Nagaishi, H.; Takeshita, Y.
626 Combustion Characteristics of Droplets Composed of Light Cycle Oil and Diesel Light
627 Oil in a Hot-Air Chamber. *Fuel* **2003**, *82* (3), 319–330. https://doi.org/10.1016/S0016-
628 2361(02)00276-4.

629 (27) Dino Imhof, Haruhiko Aoyagi, Hiroshi Tajima, K. T. Combustion and Emission
630 Formation of Gasoil and LCO (Light Cycle Oil) Water-in-Fuel Emulsions in Nitrogen
631 Enriched Air. In *Proceedings of the 8th International Conference on Modeling and*
632 *Diagnostics for Advanced Engine Systems*; 2012; pp 188–193.

633 (28) Tashima, H.; Tsuru, D. Combustion Prediction of Marine Residual Oil of Low Ignitibility
634 on Two-Component Fuel Model. *SAE Tech. Pap.* **2014**, *2014-Octob*.
635 https://doi.org/10.4271/2014-01-2556.

636 (29) Takagi, M.; Kawauchi, S.; Imai, Y.; 614 Mitsui, Y.; Aoki, G.; Hayashi, T. Numerical
637 Analysis of Evaporation Characteristics of Low Ignitability Fuel. The 24th ILASS-Japan
638 Symposium, Kobe, December 17-18, 2015; pp 192-197

639 (30) Zhang, H.; Zhu, X.; Chen, X.; Miao, P.; Yang, C.; Li, C. Fluid Catalytic Cracking of
640 Hydrogenated Light Cycle Oil for Maximum Gasoline Production: Effect of Catalyst

641 Composition. *Energy and Fuels* **2017**, *31* (3), 2749–2754.
642 https://doi.org/10.1021/acs.energyfuels.7b00185.

643 (31) Takagi, M.; Imai, Y. Evaluation of Ignitability Index and Effect of Pilot Injection on
644 Ignition Characteristics of Light Cycle Oil. *Trans. Soc. Automot. Eng. Japan* **2019**, *50* (2),
645 297–302. https://doi.org/10.11351/jsaeronbun.50.297.

646 (32) Nomura, H.; Murakoshi, T.; Suganuma, Y.; Ujiie, Y.; Hashimoto, N.; Nishida, H.
647 Microgravity Experiments of Fuel Droplet Evaporation in Sub- and Supercritical
648 Environments. *Proc. Combust. Inst.* **2017**, *36* (2), 2425–2432.
649 https://doi.org/10.1016/j.proci.2016.08.046.

650 (33) Savitzky, A.; Golay, M. J. E. Smoothing and Differentiation of Data by Simplified Least
651 Squares Procedures. *Anal. Chem.* **1964**, *36* (8), 1627–1639.
652 https://doi.org/10.1021/ac60214a047.

653 (34) Burger, M.; Schmehl, R.; Prommersberger, K.; Schäfer, O.; Koch, R.; Wittig, S. Droplet
654 Evaporation Modeling by the Distillation Curve Model: Accounting for Kerosene Fuel
655 and Elevated Pressures. *Int. J. Heat Mass Transf.* **2003**, *46* (23), 4403–4412.
656 https://doi.org/10.1016/S0017-9310(03)00286-2.

657 (35) Makino, A.; Law, C. K. On the Controlling Parameter in the Gasification Behavior of
658 Multicomponent Droplets. *Combust. Flame* **1988**, *73*, 331–336.

659 (36) Poling, B. E.; Prausnitz, M.; John P. O'Connell. The Properties of Gases and Liquids,
660 Fifth Edition. McGraw-Hill. 2006

661

662 **TOC graphic**

663